Ultrafast Picometer-Resolved Molecular Structure Imaging by Laser-Induced High-Order Harmonics

Lixin He,[1,5] C. H. Yuen,[3] Yanqing He,[1] Siqi Sun,[1] E. Goetz,[4] Anh-Thu Le,[4] Yu Deng,[1] Chengqing Xu,[1] Pengfei Lan,[1,5,*] Peixiang Lu,[1,2,5,†] and C. D. Lin[3]

[1]*Wuhan National Laboratory for Optoelectronics and School of Physics, Huazhong University of Science and Technology, Wuhan 430074, China*
[2]*Hubei Key Laboratory of Optical Information and Pattern Recognition, Wuhan Institute of Technology, Wuhan 430205, China*
[3]*Department of Physics, Kansas State University, Manhattan, Kansas 66506, USA*
[4]*Department of Physics, University of Connecticut, Storrs, Connecticut 06269-3046, USA*
[5]*Hubei Optical Fundamental Research Center, Wuhan 430074, China*

(Received 7 January 2024; revised 23 May 2024; accepted 6 June 2024; published 10 July 2024)

Real-time visualization of molecular transformations is a captivating yet challenging frontier of ultrafast optical science and physical chemistry. While ultrafast x-ray and electron diffraction methods can achieve the needed subangstrom spatial resolution, their temporal resolution is still limited to hundreds of femtoseconds, much longer than the few femtoseconds required to probe real-time molecular dynamics. Here, we show that high-order harmonics generated by intense femtosecond lasers can be used to image molecules with few-ten-attosecond temporal resolution and few-picometer spatial resolution. This is achieved by exploiting the sensitive dependence of molecular recombination dipole moment to the geometry of the molecule at the time of harmonic emission. In a proof-of-principle experiment, we have applied this high-harmonic structure imaging (HHSI) method to monitor the structural rearrangement in NH_3, ND_3, and N_2 from one to a few femtoseconds after the molecule is ionized by an intense laser. Our findings establish HHSI as an effective approach to resolve molecular dynamics with unprecedented spatiotemporal resolution, which can be extended to trace photochemical reactions in the future.

DOI: 10.1103/PhysRevLett.133.023201

Ultrafast imaging techniques have revolutionized our ability to visualize the microscopic world. Conventional methods based on electron and x-ray diffractions have been routinely used to determine the static geometric structure of molecules with subangstrom spatial resolution [1,2], but with the temporal resolution exceeding tens of picoseconds. As the time-resolved analog of x-ray and electron diffraction, recent development of femtosecond sources of x rays and electron beams [3,4] has advanced ultrafast x-ray diffraction (UXD) [5–7], ultrafast electron diffraction (UED) [8–10], and MeV-UED [11,12] for the time-resolved measurement with hundreds of femtoseconds. Such temporal resolution, however, remains inadequate for capturing the triggering event of a transformation that occurs at the few-femtosecond timescale. Most importantly, these techniques are typically limited to large-scale facilities located at national laboratories. For long-term prospects, it is crucial to explore other approaches based on laboratory-scale tabletop sources.

Recent advances in strong-field physics have promoted the development of alternative molecular imaging approaches to study molecular dynamics with femtosecond to attosecond time resolutions. The principles of these approaches are inherent to the three-step recollision model [13,14]; i.e., an electron is first ionized by the strong laser field, subsequently accelerated in the external laser field, and finally driven back to recollide with the ion. During the recollision, the instantaneous state of the molecule is probed by the returning electron through either elastic scattering with the molecular ion or high-order harmonic generation (HHG) by electron-ion recombination. Probing the static or dynamic molecular structure from elastic electron-scattering measurement is called laser-induced electron diffraction (LIED) [15–21], a time-resolved equivalent of conventional electron diffraction, which has recently been established as an emerging approach for the ultrafast imaging of molecules.

Like LIED, HHG from each single molecule intrinsically has built-in information for extracting ultrafast molecular dynamics, since the harmonic yields are proportional to the modulus square of the recombination dipole moment at the time of harmonic emission, which, in turn, is sensitive to the molecular structures [22–36]. Besides, the underlying mapping between electron excursion times and harmonic orders also provides a way for temporal measurement with attosecond resolution [31–36]. Based on these two ideas, in this Letter, we demonstrated extraction of ultrafast structure rearrangement in molecules with the high-harmonic structure imaging (HHSI) method. Unlike LIED, experimental

harmonic spectra are obtained from the coherent superposition of harmonics from all the molecules interacting with the laser. To implement HHSI successfully, we first rely on a recent development of a machine learning (ML) reconstruction algorithm [35–37] that allows us to retrieve the angle-resolved single-molecule harmonic dipole moments from the harmonic signals measured from the aligned molecules. Note that other retrieval algorithms have been explored by Wang *et al.* [38] and others [39] with different degrees of success. These angle-fixed single-molecule harmonic dipole moments, in principle, can be compared with theoretical calculations directly. Here, our goal is to use HHSI to extract the molecular structure parameters from these complex single-molecule harmonic dipole moments. Prior studies have shown that harmonic yields generated from isotopes are slightly different, with the heavier molecules having higher harmonic yields [31–33,40,41]. This is understood in terms of the motion of the nuclear wave packet of the isotope ions where the heavier isotope would move slower after the electron is ionized suddenly. These earlier studies (see below for details) do not offer a method to directly extract nuclear positions. Thus, to use HHSI, in the second step, we need to develop a new revised quantitative rescattering (QRS) model for HHG, incorporating nuclear motion, to provide the theoretical basis for extracting molecular structures from the retrieved single-molecule harmonic dipoles. Utilizing the HHSI method, we successfully reconstructed the structural changes of NH_3, ND_3, and N_2 occurring within a few femtoseconds after ionization with an unprecedented sub-picometer spatial resolution. All the reconstruction results are in good agreement with our quantum chemistry (QC) simulations. Thus, the HHSI method, besides UED, UXD, and LIED, provides an alternative tool for ultrafast imaging of molecular dynamics in chemical and biological processes.

We first demonstrate HHSI to monitor the structural rearrangement in NH_3 molecule after ionization. The principle of probing ultrafast structural dynamics in NH_3 with HHSI is sketched in Fig. 1(a). For the neutral NH_3, it has a pyramidal shape with a H—N—H bond angle of $\Phi_{HNH} = 107.23°$ at the minimum of the potential energy curve of its ground electronic state $\tilde{X}^1A_1'$. When exposed to an intense external laser field, strong-field ionization launches an electron into the continuum and simultaneously creates a nuclear wave packet on the ground state potential surface of the NH_3^+ cation ($\tilde{X}^2A_2''$). The nuclear wave packet then evolves along the NH_3^+ potential surface, manifesting as a structural transformation from the pyramidal configuration to the planar equilibrium geometry of NH_3^+ cation, as illustrated in Fig. 1(a). In HHG, the pyramidal-to-planar transition is probed by the recolliding electron, which is driven back by the laser field to recombine with the parent ion at different time delays after ionization, with the instantaneous structural information imprinted in the emitted harmonic radiation.

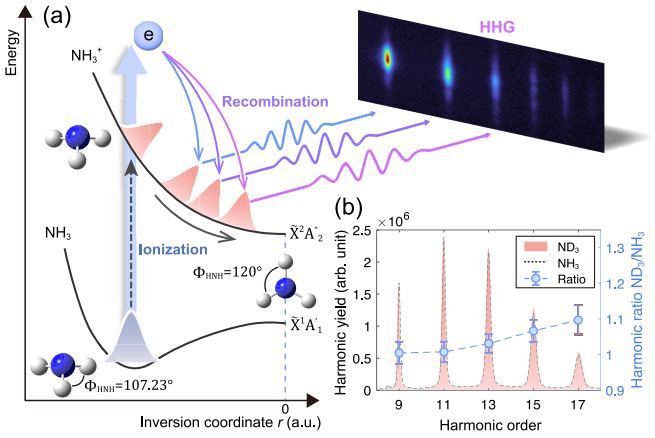

FIG. 1. (a) Scheme of probing ultrafast structural dynamics in NH_3 with HHSI. (b) High-harmonic spectra of NH_3 (dashed line) and ND_3 (shaded area) measured in the 800 nm driving field. Blue circles with a dashed line plot the harmonic yield ratios between ND_3 and NH_3.

Previously, the effect of nuclear dynamics (or structural change) on HHG has been theoretically described in [31], where the harmonic dipole moment is given by $D(\omega,\theta) = C[\Delta t(\omega)]D_{\text{fixed}}(\omega,\theta,\overrightarrow{Q_0})$. Here, $D_{\text{fixed}}(\omega,\theta,\overrightarrow{Q_0})$ is the harmonic dipole moment obtained at the initial structural geometry $\overrightarrow{Q_0}$ of the NH_3^+ cation after sudden ionization. $C(\Delta t) = \int \chi(R,0)\chi(R,\Delta t)dR$ is the nuclear autocorrelation function that denotes the overlap integral of the initial and time-dependent nuclear wave packets of the NH_3^+ cation, and Δt is the excursion time of the electron between ionization and recombination. In this model, the nuclear dynamics is separated from the electronic response by the Born-Oppenheimer approximation. The influence of the nuclear motion on the recombination dipole matrix elements of HHG is also neglected. As a consequence, the resulting harmonic intensity is approximately proportional to the squared modulus of the nuclear autocorrelation function $|C(\Delta t)|^2$. This model has been used to study the nuclear dynamics in the molecular cation from the high-harmonic spectra of two isotopes, since the different isotopes possess different nuclear motions, which will lead to an amplitude difference in the harmonic spectra of the two isotopes [see also Fig. 1(b) in this work]. By analyzing the amplitude modulation in HHG from isotopic molecules, the intracycle nuclear dynamics has been theoretically predicted to interpret experimental spectra of a H_2/D_2 [32,33,40,41] pair, as well as a CH_4/CD_4 [32,33] pair and a NH_3/ND_3 [33,42,43] pair. However, based on the autocorrelation functions, the HHG measurements can provide only partial evidence of nuclear dynamics of the complex polyatomic molecules due to large nuclear degrees of freedom. A direct imaging of the nuclear structure is not available.

In the following, we demonstrate that a direct imaging of the nuclear dynamics in NH_3 molecule is achieved by using

the HHSI method. Different from previous works [31–33,41–43], our scheme is based on a revised QRS model for molecular HHG, where the induced dipole moment for each harmonic order is approximated as (for more theoretical details, see [44])

$$D(\omega,\theta,\phi) \propto \sqrt{N(\theta,\phi)}d[\omega,\theta,\phi;\vec{Q}(\Delta t)]. \quad (1)$$

Here, $N(\theta,\phi)$ is the ionization probability of the molecule, and $d[\omega,\theta,\phi;\vec{Q}(\Delta t)]$ is the recombination dipole moment with $\vec{Q}(\Delta t)$ being the instantaneous nuclear geometry at the recombination moment of the harmonic ω. In Eq. (1), the variation of the recombination dipole moment induced by the nuclear motion is revealed. The sensitive dependence of the angle-resolved recombination dipole moments on the molecular geometry is at the heart of our reconstruction scheme, which is lacking in the previous model [31].

To extract the molecular structure, the first important ingredient of our scheme is the retrieval of the fixed-in-space single-molecule harmonic dipole moments from the measured HHG signals of aligned molecules. In our experiment, we first employed a stretched (∼160 fs) linearly polarized 800 nm laser pulse with moderate intensity ($\sim 0.6\times10^{13}$ W/cm^2) to align the NH_3 molecule ensemble in space. Another, much shorter (35 fs) and delayed 800 nm near-infrared laser pulse with higher intensity ($\sim 0.95\times10^{14}$ W/cm^2) and the same polarization was used to interact with the aligned molecules to generate high-order harmonics (for more experimental details, see [44]). Figure 2(a) displays the time-dependent alignment factor $\langle\cos^2\theta\rangle(t)$ around the first rotational revival of NH_3, extracted according to the experimental parameters [56]. Figures 2(b)–2(d) show the harmonic intensities measured at the same time delays as in Fig. 2(a), for the 11th (H11), 13th (H13), and 15th (H15) harmonics, respectively. The intensity of each harmonic order is found to present a minimum (maximum) when the C_{3v} symmetry axis of the NH_3 molecule is aligned perpendicular (parallel) to the polarization direction of the driving pulse. This result is consistent with the symmetry of the highest occupied molecular orbital (HOMO) of NH_3. The distinct local minima and maxima at the time of rotational revival also indicate that our experiment dominantly measured the signals from the isolated molecules rather than the clusters [42].

By using the advanced ML algorithm developed in [37], we were able to reconstruct the single-molecule harmonic dipole moment for each fixed-in-space alignment angles from the measured alignment-averaged harmonic spectra. For the one-dimensional alignment created by the linearly polarized alignment pulse, the retrieved single-molecule harmonic dipole moment for each alignment angle θ should be the result averaged over the up and down orientations as well as the rotation angle ϕ about the C_{3v} axis [see Fig. 2(e)], i.e.,

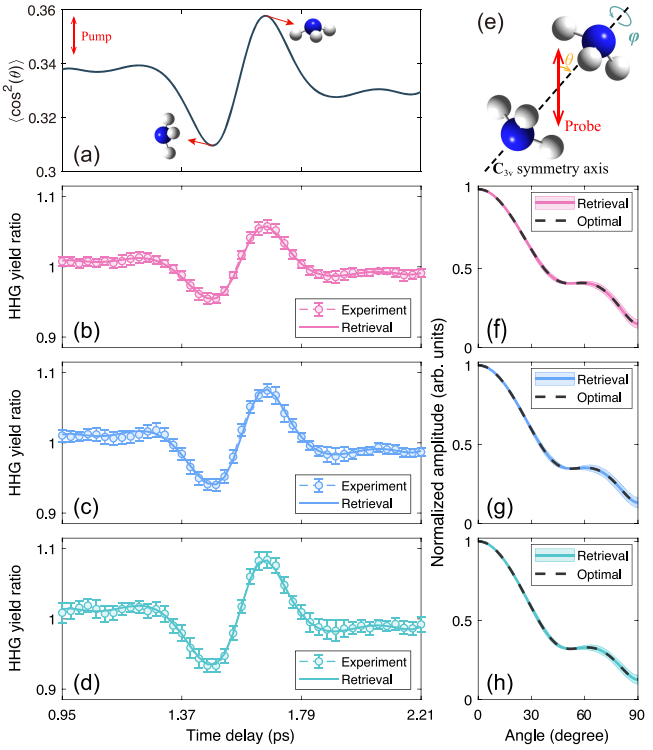

FIG. 2. (a) The time-dependent alignment factor $\langle\cos^2\theta\rangle(t)$ of NH_3 extracted from the experimental HHG data. (b)–(d) HHG yields of H11–H15 measured around the alignment revival of NH_3 in the 800 nm driving field. Here, the polarization of driving pulse is parallel to that of the alignment pulse. The HHG yields of each harmonic order have been normalized by the results of the isotropic alignment. (e) Geometry of the one-dimensional molecular alignment of NH_3 in the experiment. (f)–(h) Angle-resolved single-molecule harmonic dipole amplitudes (solid lines) of H11–H15 retrieved from the experimental data in (b) and (c) with the ML algorithm. Dashed lines display the theoretical results calculated with the optimized geometric structure of NH_3^+ cation for comparison.

$$\overline{D}(\omega,\theta) = \frac{1}{4\pi}\int_0^{2\pi}[D(\omega,\theta,\phi) + D(\omega,\pi+\theta,\phi)]d\phi. \quad (2)$$

Figures 2(f)–2(h) show the retrieved dipole amplitude $|\bar{D}(\theta)|$ of H11–H15 (solid lines), respectively. Since in our reconstruction we are interested only in the angle dependence of $|\bar{D}(\theta)|$, the retrieved $|\bar{D}(\theta)|$ for each order has been normalized with respect to the retrieved result at $\theta = 0°$. By convoluting the retrieved single-molecule dipole moment with the molecular alignment distribution in our experiment, we have accurately reproduced the experimental HHG signals shown in Figs. 2(b)–2(d) (see the solid lines). Such an excellent agreement proves the accuracy and validity of our reconstruction method (more test details can also be seen in [44]).

With the single-molecule harmonic dipole moments retrieved, the geometric configuration of NH_3 then can be determined by optimizing the structure parameters R_{NH}

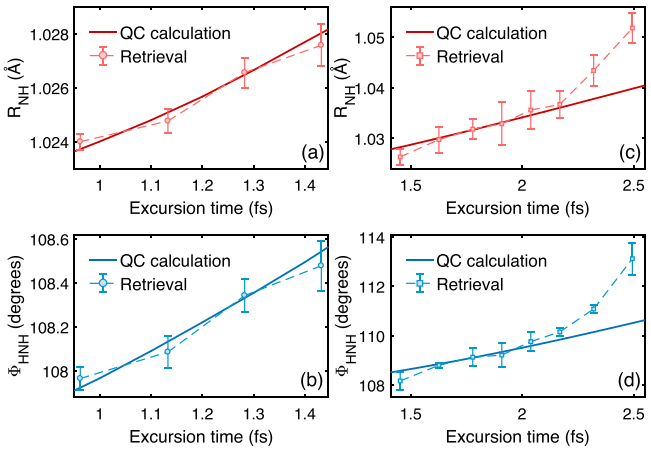

FIG. 3. (a) The N—H bond length R_{NH} extracted (circles with dashed line) as a function of the excursion times of harmonics H11–H17 in the 800 nm driving field. The solid line shows the result of the QC calculations for comparison. (b) The same as (a), but for the result of H—N—H bond angle Φ_{HNH}. (c),(d) The same as (a) and (b), respectively, but for H17–H31 in the 1300 nm driving field.

and Φ_{HNH} such that the theoretical dipole moments calculated by Eqs. (1) and (2) agree best with the experimental retrievals [see dashed lines in Figs. 2(f)–2(h)]. Note that, in our reconstruction, while only the dipole amplitudes were used, our ML algorithm can also retrieve the harmonic dipole phases. We have checked that the retrieved dipole phases also agree well with the calculations with the molecular geometry optimized by the dipole amplitudes (see [44]). Repeating the reconstruction for each harmonic order, a real-time measurement of the ultrafast structural transformation was ultimately achieved upon the unique relationship between the harmonic order and the excursion time of the electron in the continuum. During the HHG process, there are two trajectories per optical half cycle, which are referred to as the short and long trajectories, contributing to each individual harmonic order [13,14,30,33,57]. To obtain a one-to-one mapping between the excursion time and harmonic order, phase matching in the experiment has been achieved such that only short-trajectory electrons contribute to each harmonic. Figures 3(a) and 3(b) display the extracted bond length R_{NH} and bond angle Φ_{HNH} as a function of the excursion times of H11–H17. As shown, both R_{NH} and Φ_{HNH} increase with time, which is in agreement with the expected pyramidal-to-planar transition. To verify the retrieved results from the experiment, we have also performed QC calculations to obtain how the molecular structure of NH_3 changes with time. As shown in Figs. 3(a) and 3(b), the R_{NH} and Φ_{HNH} obtained from QC calculations (solid lines) are in quantitative agreement with our reconstructions.

We have also performed HHG experiment with a longer 1300 nm driving laser to expand the time window of measurement. In our experiment, the 1300 nm laser intensity is about 0.4×10^{14} W/cm^2. Figure S6 in Supplemental Material [44] shows the measured HHG spectra versus the time delay for H19, H25, and H29 and the retrieved angle-resolved single-molecule harmonic dipole amplitudes. Following the same procedure, we then extracted R_{NH} and Φ_{HNH} for different excursion times of H17–H31 over a longer temporal range as shown in Figs. 3(c) and 3(d). These results are in good agreement with QC calculations (sold lines) except for H29 and H31 that are near the cutoff region. In this region, the long trajectory starts to play a role in the harmonic generation (see [44]). It is estimated that, using a 3200 nm midinfrared driving laser [20], the entire pyramidal-to-planar transition in NH_3^+ will be fully visualized with our method due to much longer excursion time of the electron.

Our scheme has also been used to reconstruct the structural dynamics in the isotope molecule ND_3 independently, of which a slower structural transition can be directly visualized from the reconstructions (see [44]). In addition, we also carried out HHG spectra and reconstructed the structure dynamics of N_2 molecules. In Fig. S12 in Supplemental Material [44], we show that the N—N stretch is much smaller, but they are in agreement with the QC calculation.

To demonstrate the robustness and consistency of the results obtained by the HHSI method, in Table S1 in Supplemental Material [44], we tabulate the change of bond length in picometers and bond angle in degrees, versus the recombination times from 0.96 to 2.49 fs after ionization, for NH_3 in the 800 and 1300 nm lasers. The time interval between successive odd harmonics is about 150 as (not constant due to attochirp), while the bond length changes at a fraction of one picometer. It is interesting that such a minute change of mean nuclear separation in such a short time can be captured by the harmonic signals. Among NH_3, ND_3, and N_2, Table S1(a)–(c) shows that each molecule stabilizes by stretching the internuclear separation after ionization, and the heavier the molecule, the slower the separation. This can be clearly seen from Fig. 4, which plots the retrieved bond length changes of these three molecules as a function of the recombination times of the harmonics. However, the mass alone is not the only factor for the rate of separation. Note that these three molecules have bonding HOMO orbitals. In the case of an antibonding HOMO orbital like O_2, the internuclear separation would shrink upon the removal of the valence electron. In Table S1(c), we show the O—O bond length contraction obtained from the QC calculations. We have not carried out the HHG experiment on O_2, but we obtained bond contraction from QC calculations. We noted that the QC results at later times are in good agreement with the contraction extracted from earlier LIED experiments [15]. The spatial resolution in LIED was estimated to be about 5 pm such that the change of bond length in N_2 was

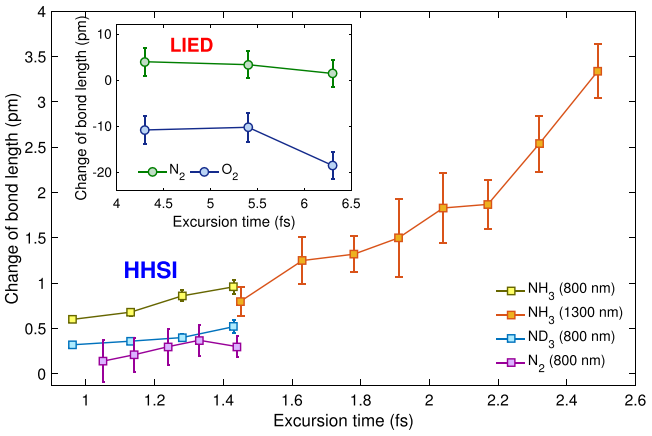

FIG. 4. Species-dependent subpicometer-level changes of molecular bond lengths with attosecond temporal resolution extracted from experimental high-order harmonic spectra using the HHSI. The inset shows the LIED results of N_2 (green circles) and O_2 (blue circles) taken from Ref. [15] for comparison.

not resolved (see the inset in Fig. 4). In Fig. 4, for N_2, the N—N distance changes for the short times from 1.05 to 1.44 fs obtained from HHSI are consistent with the distance changes at longer times from 4.30 to 6.30 fs obtained from LIED but with spatial resolution better than one picometer. In addition to the experimental reconstructions, we have also checked the sensitivity of harmonic dipole moments to molecular geometry. As shown in Fig. S14 in Supplemental Material [44], the subpicometer change in the molecular geometry can lead to considerable variations in the harmonic dipole moments as well as the HHG signals, which further verifies the subpicometer resolution capability of our HHSI method.

Finally, we remark that, in general, multiple orbitals could contribute to molecular HHG [26,27,30,34–36], especially at higher laser intensity. For the present HHSI to work, multiple-orbital effects, however, should be avoided. When multiple orbitals contribute to the measured harmonics, a nuclear wave packet with complex amplitudes for individual ionic states is generated. To extract the whole nuclear wave packet, one has to disentangle the contribution of harmonics from each orbital experimentally, which will dramatically complicate the reconstruction, since contributions from multiple orbitals are added coherently. In our experiment, we chose the laser intensity such that the contribution of the HOMO-1 of NH_3 can be neglected (see [44]). For N_2, HOMO and HOMO-1 orbitals both contribute to harmonics in the cutoff region [26,37]. In this work, only the harmonics in the plateau were used to do the retrieval.

In conclusion, we have demonstrated the HHSI technique to directly image the ultrafast structural rearrangement in molecules after strong-field ionization with subpicometer spatial and attosecond temporal resolutions. This is made possible by two new developments. First, with the help of a modern ML algorithm, we are able to successfully retrieve single-molecule recombination dipole at each fixed-in-space angle from experimental harmonic spectra taken with partially aligned molecules. These energy- and angle-dependent dipole moments are sensitive to the molecular structure. Second, a new HHG theory for molecules including nuclear motion was formulated [see Eq. (1) and [44]] which relates the retrieved dipole moment to molecular structure parameters at the time of recombination. Starting with molecules at the ground state, we have demonstrated that minute bond changes on the order of subpicometers within tens to hundreds of attoseconds can be extracted from the measured harmonic spectra, as presented in Table S1 in Supplemental Material [44].

We comment that, while the HHSI and LIED have been limited to probing the molecular dynamics only at the first sub- to few femtoseconds after one electron has been quickly removed, both methods do provide unprecedentedly high spatial and temporal resolutions, and the results, as shown in Table S1 and Fig. 4, do nicely reveal that the early molecular dynamics depends on the molecular structures as well as the isotopes. Looking ahead, we anticipate that both HHSI and LIED may serve as a potential approach for probing real-space molecular structures, particularly in dynamic systems initiated by a pump pulse. In the pump-probe experiment, the extreme picometer-attosecond spatial-temporal imaging from HHSI is not essential for probing a dynamic system where lesser resolutions would be adequate. In such cases, the harmonic signals obtained at each time delay can serve as additional data to extract angle-resolved single-molecule transition dipoles using the same ML method employed here. Potential applications of HHSI would include the probing of proton transfer, conical intersections, structural isomerization, and the ring-opening reaction of molecules.

This work was supported by National Key Research and Development Program of China (Grant No. 2023YFA1406800), National Natural Science Foundation of China (Grants No. 12225406, No. 12074136, No. 11934006, and No. 12021004). C. D. L. and C. H. Y. were supported by Chemical Sciences, Geosciences and Biosciences Division, Office of Basic Energy Sciences, Office of Science, U.S. Department of Energy under Grant No. DE-FG02-86ER13491. Work by E. G. and A.-T. L. was supported by the U.S. Department of Energy, Office of Science, Office of Basic Energy Sciences under Grant No. DE-SC0023192. The computing work from HUST was supported by the Public Service Platform of High Performance Computing provided by Network and Computing Center of Huazhong University of Science and Technology (HUST).

L. H., C. H. Y., and Y. H. contributed equally to this letter.

*Contact author: pengfeilan@hust.edu.cn
†Contact author: lupeixiang@hust.edu.cn

[1] A. H. Zewail, Femtochemistry: Atomic-scale dynamics of the chemical bond, J. Phys. Chem. A **104**, 5660 (2000).
[2] F. Carbone, O.-H. Kwon, and A. H. Zewail, Dynamics of chemical bonding mapped by energy-resolved 4D electron microscopy, Science **325**, 181 (2009).
[3] B. W. J. McNeil and N. R. Thompson, X-ray free-electron lasers, Nat. Photonics **4**, 814 (2010).
[4] F. Carbone, P. Musumeci, O. J. Luiten, and C. Hebert, A perspective on novel sources of ultrafast electron and x-ray pulses, Chem. Phys. **392**, 1 (2012).
[5] C. Rischel, A. Rousse, I. Uschmann, P.-A. Albouy, J.-P. Geindre, P. Audebert, J.-C. Gauthier, E. Fröster, J.-L. Martin, and A. Antonetti, Femtosecond time-resolved x-ray diffraction from laser-heated organic films, Nature (London) **390**, 490 (1997).
[6] H. Ihee, M. Lorenc, T. K. Kim, Q. Y. Kong, M. Cammarata, J. H. Lee, S. Bratos, and M. Wulff, Ultrafast x-ray diffraction of transient molecular structures in solution, Science **309**, 1223 (2005).
[7] H. N. Chapman *et al.*, Femtosecond diffractive imaging with a soft-x-ray free-electron laser, Nat. Phys. **2**, 839 (2006).
[8] R. Srinivasan, V. A. Lobastov, C.-Y. Ruan, and A. H. Zewail, Ultrafast electron diffraction (UED), Helv. Chim. Acta **86**, 1761 (2003).
[9] B. J. Siwick, J. R. Dwyer, R. E. Jordan, and R. J. D. Miller, An atomic-level view of melting using femtosecond electron diffraction, Science **302**, 1382 (2003).
[10] J. Yang *et al.*, Imaging CF_3I conical intersection and photodissociation dynamics with ultrafast electron diffraction, Science **361**, 64 (2018).
[11] E. Champenois *et al.*, Conformer-specific photochemistry imaged in real space and time, Science **374**, 178 (2021).
[12] M. Centurion, T. Wolf, and J. Yang, Ultrafast imaging of molecules with electron diffraction, Annu. Rev. Phys. Chem. **73**, 21 (2022).
[13] P. B. Corkum, Plasma perspective on strong field multiphoton ionization, Phys. Rev. Lett. **71**, 1994 (1993).
[14] M. Lewenstein, P. H. Balcou, M. Ivanov, A. L'Huillier, and P. B. Corkum, Theory of high-harmonic generation by low-frequency laser fields, Phys. Rev. A **49**, 2117 (1994).
[15] I. Blaga, J. Xu, A. D. DiChiara, E. Sistrunk, K. Zhang, P. Agostini, T. A. Miller, L. F. DiMauro, and C. D. Lin, Imaging ultrafast molecular dynamics with laser-induced electron diffraction, Nature (London) **483**, 194 (2012).
[16] B. Wolter *et al.*, Ultrafast electron diffraction imaging of bond breaking in diionized acetylene, Science **354**, 308 (2016).
[17] J. Xu, C. I. Blaga, K. Zhang, Y. H. Lai, C. D. Lin, T. A. Miller, P. Agostini, and L. F. DiMauro, Diffraction using laser-driven broadband electron wave packets, Nat. Commun. **5**, 4635 (2014).
[18] K. Amini *et al.*, Imaging the Renner-Teller effect using laser-induced electron diffraction, Proc. Natl. Acad. Sci. U.S.A. **116**, 8173 (2019).
[19] M. G. Pullen *et al.*, Influence of orbital symmetry on diffraction imaging with rescattering electron wave packets, Nat. Commun. **7**, 11922 (2016).
[20] B. Belsa *et al.*, Laser-induced electron diffraction of the ultrafast umbrella motion in ammonia, Struct. Dyn. **8**, 014301 (2021).
[21] M. G. Pullen *et al.*, Imaging an aligned polyatomic molecule with laser induced electron diffraction, Nat. Commun. **6**, 7262 (2015).
[22] C. D. Lin, A. T. Le, Z. Chen, T. Morishita, and R. Lucchese, Strong-field rescattering physics—Self-imaging of a molecule by its own electrons, J. Phys. B **43**, 122001 (2010).
[23] J. Itatani, J. Levesque, D. Zeidler, H. Niikura, H. Pépin, J. C. Kieffer, P. B. Corkum, and D. M. Villeneuve, Tomographic imaging of molecular orbitals, Nature (London) **432**, 867 (2004).
[24] S. Haessler *et al.*, Attosecond imaging of molecular electronic wavepackets, Nat. Phys. **6**, 200 (2010).
[25] C. Vozzi, M. Negro, F. Calegari, G. Sansone, M. Nisoli, S. De Silvestri, and S. Stagira, Generalized molecular orbital tomography, Nat. Phys. **7**, 822 (2011).
[26] B. McFarland, J. P. Farrell, P. H. Bucksbaum, and M. Gühr, High harmonic generation from multiple orbitals in N_2, Science **322**, 1232 (2008).
[27] O. Smirnova, Y. Mairesse, S. Patchkovskii, N. Dudovich, D. Villeneuve, P. Corkum, and M. Yu. Ivanov, High harmonic interferometry of multi-electron dynamics in molecules, Nature (London) **460**, 972 (2009).
[28] N. L. Wagner, A. Wüest, I. P. Christov, T. Popmintchev, X. Zhou, M. M. Murnane, and H. C. Kapteyn, Monitoring molecular dynamics using coherent electrons from high harmonic generation, Proc. Natl. Acad. Sci. U.S.A. **103**, 13279 (2006).
[29] W. Li, X. Zhou, R. Lock, S. Patchkovskii, A. Stolow, H. C. Kapteyn, and M. M. Murnane, Time-resolved dynamics in N_2O_4 probed using high harmonic generation, Science **322**, 1207 (2008).
[30] A. Camper, A. Ferré, V. Blanchet, D. Descamps, N. Lin, S. Petit, R. Lucchese, P. Salières, T. Ruchon, and Y. Mairesse, Quantum-path-resolved attosecond high-harmonic spectroscopy, Phys. Rev. Lett. **130**, 083201 (2023).
[31] M. Lein, Attosecond probing of vibrational dynamics with high-harmonic generation, Phys. Rev. Lett. **94**, 053004 (2005).
[32] S. Baker, J. S. Robinson, C. A. Haworth, H. Teng, R. A. Smith, C. C. Chirilă, M. Lein, J. W. G. Tisch, and J. P. Marangos, Probing proton dynamics in molecules on an attosecond time scale, Science **312**, 424 (2006).
[33] P. Lan *et al.*, Attosecond probing of nuclear dynamics with trajectory-resolved high-harmonic spectroscopy, Phys. Rev. Lett. **119**, 033201 (2017).
[34] P. M. Kraus *et al.*, Measurement and laser control of attosecond charge migration in ionized iodoacetylene, Science **350**, 790 (2015).
[35] L. He *et al.*, Filming movies of attosecond charge migration in single molecules with high harmonic spectroscopy, Nat. Commun. **13**, 4595 (2022).
[36] L. He *et al.*, Attosecond probing and control of charge migration in carbon-chain molecule, Adv. Opt. Photonics **5**, 056001 (2023).
[37] S. Sun, Y. He, L. He, J. Hu, P. Lan, and P. Lu, Iterative projection algorithm for retrieval of angle-resolved

single-molecule dipoles from high-harmonic spectra, Phys. Rev. A **107**, 033105 (2023).
[38] X. Wang, A. T. Le, Z. Zhou, H. Wei, and C. D. Lin, Theory of retrieving orientation-resolved molecular information using time-domain rotational coherence spectroscopy, Phys. Rev. A **96**, 023424 (2017).
[39] B. Wang, Y. He, X. Zhao, L. He, P. Lan, P. Lu, and C. D. Lin, Retrieval of full angular- and energy-dependent complex transition dipoles in the molecular frame from laser-induced high-order harmonic signals with aligned molecules, Phys. Rev. A **101**, 063417 (2020).
[40] S. Baker *et al.*, Dynamic two-center interference in high-order harmonic generation from molecules with attosecond nuclear motion, Phys. Rev. Lett. **101**, 053901 (2008).
[41] H. Mizutani, S. Minemoto, Y. Oguchi, and H. Sakai, Effect of nuclear motion observed in high-order harmonic generation from D_2/H_2 molecules with intense multi-cycle 1300 nm and 800 nm pulses, J. Phys. B **44**, 081002 (2011).
[42] P. M. Kraus and H. J. Wörner, Attosecond nuclear dynamics in the ammonia cation: Relation between high-harmonic and photoelectron spectroscopies, Chem. Phys. Chem. **14**, 1445 (2013).
[43] J. Förster and A. Saenz, Theoretical study of the inversion motion of the ammonia cation with subfemtosecond resolution for high-harmonic spectroscopy, Chem. Phys. Chem. **14**, 1438 (2013).
[44] See Supplemental Material at http://link.aps.org/supplemental/10.1103/PhysRevLett.133.023201 for more information about the experimental results and the numerical simulations, which includes Refs. [45–55].
[45] A. T. Le, R. R. Lucchese, S. Tonzani, T. Morishita, and C. D. Lin, Quantitative rescattering theory for high-order harmonic generation from molecules, Phys. Rev. A **80**, 013401 (2009).
[46] C. D. Lin, A. T. Le, C. Jin, and H. Wei, *Attosecond and Strong-Field Physics: Principles and Applications* (Cambridge University Press, Cambridge, England, 2018).
[47] C. D. Lin, A. T. Le, C. Jin, and H. Wei, Elements of the quantitative rescattering theory, J. Phys. B **51**, 104001 (2018).
[48] X. M. Tong, Z. X. Zhao, and C. D. Lin, Theory of molecular tunneling ionization, Phys. Rev. A **66**, 033402 (2002).
[49] N. Douguet, S. Fonseca dos Santos, M. Raoult, O. Dulieu, A. E. Orel, and V. Kokoouline, Theory of radiative electron attachment to molecules: Benchmark study of CN^-, Phys. Rev. A **88**, 052710 (2013).
[50] E. S. Chang and U. Fano, Theory of electron-molecule collisions by frame transformations, Phys. Rev. A **6**, 173 (1972).
[51] S. Zhao, J. Xu, C. Jin, A.-T. Le, and C. D. Lin, Effect of orbital symmetry on the orientation dependence of strong field tunnelling ionization of nonlinear polyatomic molecules, J. Phys. B **44**, 035601 (2011).
[52] I. F. Galván *et al.*, OpenMolcas: From source code to insight, J. Chem. Theory Comput. **15**, 5925 (2019).
[53] R. A. Kendall, T. H. Dunning Jr, and R. J. Harrison, Electron affinities of the first-row atoms revisited. Systematic basis sets and wave functions, J. Chem. Phys. **96**, 6796 (1992).
[54] F. A. Gianturco, R. R. Lucchese, and N. Sanna, Calculation of low-energy elastic cross sections for electron-CF_4 scattering, J. Chem. Phys. **100**, 6464 (1994).
[55] A. P. Natalense and R. R. Lucchese, Cross section and asymmetry parameter calculation for sulfur 1s photoionization of SF_6, J. Chem. Phys. **111**, 5344 (1999).
[56] Y. He, L. He, P. Wang, B. Wang, S. Sun, R. Liu, B. Wang, P. Lan, and P. Lu, Measuring the rotational temperature and pump intensity in molecular alignment experiments via high harmonic generation, Opt. Express **28**, 21182 (2020).
[57] L. He, P. Lan, Q. Zhang, C. Zhai, F. Wang, W. Shi, and P. Lu, Spectrally resolved spatiotemporal features of quantum paths in high-order-harmonic generation, Phys. Rev. A **92**, 043403 (2015).